Effect of the quark-gluon vertex on dynamical chiral symmetry breaking

M. Atif Sultan,[1,*] Khépani Raya,[2,3,†] Faisal Akram,[1,‡] Adnan Bashir,[4,§] and Bilal Masud[1,‖]

[1]*Centre For High Energy Physics, University of the Punjab, Lahore (54590), Pakistan*
[2]*School of Physics, Nankai University, Tianjin 300071, China*
[3]*Instituto de Ciencias Nucleares, Universidad Nacional Autónoma de Mexico, Apartado Postal 70-543, C.P. 04510, CDMX, Mexico*
[4]*Instituto de Física y Matemáticas, Universidad Michoacana de San Nicolás de Hidalgo, Edificio C-3, Ciudad Universitaria, C.P. 58040, Morelia, Michoacán, Mexico*

(Received 2 January 2021; accepted 8 February 2021; published 25 March 2021)

In this work, we investigate how the details of the quark-gluon interaction vertex affect the quantitative description of chiral symmetry breaking through the gap equation for quarks. We start from two gluon propagator models widely used in literature and constructed in direct connection with our gradually improved understanding of infrared quantum chromodynamics coupled with its exact one-loop limit. The gap equation is then solved by employing a variety of vertex *Ansätze*, which have been constructed in order to implement some of the key aspects of quantum chromodynamics, namely, multiplicative renormalizability of the quark propagator, gauge invariance, matching with perturbation theory in the weak coupling regime, independence from unphysical kinematic singularities as well as manifestly correct transformation properties under charge conjugation and parity operations. On general grounds, all truncation schemes exhibit the same qualitative and quantitative pattern of chiral symmetry breaking, ensuring the overall robustness of this approach and its potentially reliable description of the hadron spectrum and properties.

DOI: 10.1103/PhysRevD.103.054036

I. INTRODUCTION

If quantum chromodynamics (QCD) is the underlying theory of strong interactions, we expect all hadronic observables to be calculable from the complete knowledge of the corresponding Green functions. There is an infinite set of integral field theoretic equations which describe these n-point functions in a coupled and highly nonlinear manner. These are the well-known Schwinger-Dyson equations (SDEs) [1–3]. Their structure is such that any n-point function is related to at least one higher order Green function; the two-point one-particle irreducible (1PI) Green functions (propagators) are related to the three-point functions (vertices), which in turn are entangled with the four-point functions (scattering kernels), *ad infinitum*. In a general formalism, not limited to the perturbative domain, this infinite set must be truncated by introducing physically reliable model(s) of some suitable set of Green functions before a solution becomes tractable. The most favorite choice, which lies on the borderline of a daunting computational complexity while still maintaining predictable exploration of hadronic physics, is to model the three-point vertices whether they be quark-photon or quark-gluon interactions [4–19]. It is natural to demand any truncation of SDEs to resemble the true dynamics of quarks and gluons to the fullest extent possible, while successfully describing the observable degrees of freedom, namely, mesons and baryons. Several reviews describe the tremendous success of the SDE approach to our continually improved understanding of QCD, hadron spectrum and properties, see for example [20–26]. Ideally, we can impose the following restrictions on the quark-gluon vertex (QGV) which enters the gap equation directly and also constrains the kernel of the Bethe-Salpeter equation accordingly [27–29]:

(i) The QGV must satisfy the Slavnov-Taylor identity (STI) [30,31]. This implies that the requirement of gauge invariance fixes the longitudinal part of the quark-gluon interaction, [19]. Its Abelian counterpart is generally known as the Ball-Chiu vertex [4]. For most practical purposes and Abelian-like truncations, one can start from the Ball-Chiu construction as the longitudinal one and push the remaining information in the rich transverse part of it.

(ii) The transverse part is tightly constrained by the requirements of the generalized Landau-Khalatnikov-Fradkin transformations (LKFT) [32–34] and the transverse Takahashi identities (TTI) [9,35–40].

(iii) It should reduce to its perturbation theory Feynman expansion. Note that a truncation scheme of the complete set of SDEs, which maintains multiplicative

*atifsultan.chep@pu.edu.pk
†khepani@nankai.edu.cn
‡faisal.chep@pu.edu.pk
§adnan.bashir@umich.mx
‖bilalmasud.chep@pu.edu.pk

renormalizability (MR) of the quark propagator and gauge invariance at every level of approximation, is perturbation theory. Therefore, we expect physically meaningful solutions of the SDEs to agree with perturbative results in the weak coupling regime [18,41–45].

(iv) It should transform correctly under the discrete symmetries of charge, conjugation, parity and time reversal (C, P and T).

(v) It should be free of any kinematic singularities.

(vi) It should lead to physical observables which are strictly gauge independent [6–9].

However, the fact remains that any truncation of the SDEs can only be considered sensible if it is consistently able to reproduce the experimental observations pertaining to QCD and hadron physics. The leading-order symmetry-preserving rainbow-ladder (RL) truncation achieves that goal quite successfully when studying low lying mesons and baryons [46–48]. For instance, since the dynamical chiral symmetry breaking (DCSB) pattern of the pseudoscalar meson sector is governed by a close relationship between the gap equation and the Bethe-Salpeter kernel, supplied by the axial vector Ward-Green-Fradkin-Takahashi identity (WGFTI) [49], it is not a surprise that the RL truncation provides an excellent description of these mesons.

For the gap equation, the usual practice is to employ models for the gluon propagator, constructed by making connections with lattice results, perturbation theory as well as hadron phenomenology, instead of simultaneously solving the corresponding SDEs. A popular choice is the well-known Maris-Tandy (MT) model [50]. This model is composed of two terms: an ultraviolet term, fixed from perturbation theory, and an infrared enhancement term whose strength is typically determined from the chiral quark condensate. Notice that the MT model was put forward before the SDE prediction for the massive gluon solution [51] which was later confirmed in lattice studies [52–55]. It supports a finite but infrared enhanced scalar form factor of the gluon propagator, the so-called decoupling solution. It is also in agreement with subsequent SDE and functional renormalization group results [56–63], refined Gribov-Zwanziger formalism [64–66] and the earlier suggestion of Cornwall [67]. Even if one includes the effect of dynamical quarks [68–70], the qualitative behavior of the gluon propagator remains the same and feeds expected physics back into the gap equation [71]. Those facets of the gluon propagator are confirmed in novel combined continuum and lattice studies [72,73]. The Qin-Chang (QC) model [28] conveniently captures these infrared qualitative features of the gluon propagator, while the connection with one-loop perturbation theory is still maintained just as it was incorporated in the MT model.

In this article, we employ the effective coupling of both the MT and the QC models in association with a set of refined *Ansätze* for the fermion-boson vertex: Ball-Chiu (BC) [4], Curtis-Pennington (*CP*) [5], Kizilersu-Pennington (KP) [11] and Bashir *et al.* (BB) [8]. For comparison with these refined vertices and the sake of completeness, we have included the results based upon the bare vertex as well.

The article is organized as follows: in Sec. II we discuss the preliminaries of the gap equation, introducing the MT and the QC models. In Sec. III, we explicitly discuss all the vertex constructions we employ, highlighting, comparing and contrasting their merits. Section IV details the algebraic expressions for the kernels of the gap equation that stem from the choice of each vertex and Sec. V contains numerical results as well as a comparative analysis. Finally, in Sec. VI, we summarize our conclusions and discuss the scope and future applications of this work.

II. GAP EQUATION: PRELIMINARIES AND THE GLUON PROPAGATOR

In order to investigate how DCSB is realized, we naturally start from the renormalized SDE for the quark propagator. This equation is depicted in Fig. 1 and can be written in the following mathematical form:

$$S^{-1}(p) = Z_2(i\gamma\cdot p + m_0) + \Sigma(p), \tag{1}$$

where $\Sigma(p)$ is the quark self-energy defined as

$$\Sigma(p) = Z_1 C_F \int_k g^2 D_{\mu\nu}(q)\gamma_\mu S(k)\Gamma_\nu(k,p). \tag{2}$$

Here $q = k - p$, $C_F = 4/3$ and $\int_k \equiv \int^\Lambda \frac{d^4k}{(2\pi)^4}$. Z_1 and Z_2 are the renormalization constants for the QGV and the quark propagator, respectively, which depend on the ultraviolet regulator (Λ) and the renormalization point (μ). This equation, also known as the *gap equation*, involves not only the full quark propagator, $S(p)$, but also the full gluon propagator, $D_{\mu\nu}(q)$, and the fully dressed QGV, $\Gamma_\nu(k,P)$. Each of these Green functions also depend on the renormalization point. However, we have not explicitly displayed this dependence for notational convenience. Moreover, they obey their own SDEs. This intricate structure yields an infinite tower of coupled equations, which must be systematically truncated in order to extract the encoded physics. Regardless of the truncation scheme, the full quark propagator, representing a Dirac particle, can be defined in terms of two scalar functions, namely the mass function, $M(p^2)$, and the quark wave function renormalization, $Z(p^2;\mu^2)$, such that

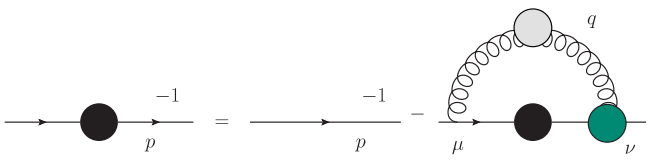

FIG. 1. SDE of the full quark propagator. The blobs represent fully-dressed propagators and vertices, which obey their own SDEs.

$$S(p;\mu) = \frac{Z(p^2;\mu^2)}{i\gamma\cdot p + M(p^2)}, \tag{3}$$

in analogy to its bare counterpart

$$S_0(p) = \frac{1}{i\gamma\cdot p + m_0},$$

where m_0 is the bare mass of the quark. Equivalent useful representations of $S(p;\mu)$ are

$$\begin{aligned} S(p;\mu) &= -i\gamma\cdot p\sigma_v(p^2;\mu^2) + \sigma_s(p^2;\mu^2), \\ S^{-1}(p;\mu) &= i\gamma\cdot pA(p^2;\mu^2) + B(p^2;\mu^2), \end{aligned} \tag{4}$$

where the dressing functions involved are interrelated as

$$\begin{aligned} \sigma_s(k^2;\mu^2) &= \frac{B(k^2;\mu^2)}{A^2(k^2;\mu^2)k^2 + B^2(k^2;\mu^2)}, \\ \sigma_v(k^2;\mu^2) &= \frac{A(k^2;\mu^2)}{A^2(k^2;\mu^2)k^2 + B^2(k^2;\mu^2)}, \end{aligned}$$

and one can easily identify

$$M(p^2) = \frac{B(p^2;\mu^2)}{A(p^2;\mu^2)}, \qquad Z(p^2;\mu^2) = \frac{1}{A(p^2;\mu^2)}.$$

Notably, multiplicative renormalizability ensures that the mass function does not depend on the renormalization point. For the simplicity of notation, we will omit displaying the μ dependence altogether. The general form of the gluon propagator is

$$D_{\mu\nu}(q) = \frac{D(q^2)}{q^2}\left[\delta_{\mu\nu} - \frac{q_\mu q_\nu}{q^2}\right] + \xi\frac{q_\mu q_\nu}{q^4}, \tag{5}$$

where $D(q^2)$ is the gluon dressing function and ξ is the covariant gauge parameter. Due to the corresponding Ward identity, the longitudinal term proportional to ξ does not get corrections at any order of perturbation theory. Hence $\xi = 0$ is an obvious first option to work with. It corresponds to the Landau gauge, which is a convenient and natural choice for several reasons. Among others, model dependent differences between various *Ansätze* for the QGV are least noticeable in this gauge [17]. Moreover, it is a covariant gauge which is readily implemented in lattice QCD simulations [74,75].

The first model of the gluon propagator employed herein is the MT interaction [50], where the effective coupling, $\alpha_s(q^2) \equiv g^2D(q^2)/4\pi$, has the following form:

$$\frac{\alpha_s(q^2)}{q^2} = \frac{\pi D}{\omega^6}q^2e^{-q^2/\omega^2} + \frac{\gamma_m\pi F(q^2)}{\frac{1}{2}\ln[\tau + (1+q^2/\Lambda_{\rm QCD}^2)^2]}, \tag{6}$$

with $F(q^2) = \{1 - e^{-q^2/[4m_t^2]}\}/q^2$, $\tau = e^2 - 1$, $\gamma_m = 12/(33 - 2N_f)$, $N_f = 4$, $m_t = 0.5$ GeV and $\Lambda_{\rm QCD} = 0.234$ GeV. The first term provides an infrared enhancement, controlled by the parameters ω and D, while the second term reproduces the one-loop renormalization group equation of QCD.

The other model choice is the QC interaction [28]:

$$\frac{\alpha_s(q^2)}{q^2} = \frac{2\pi D}{\omega^4}e^{-q^2/\omega^2} + \frac{\gamma_m\pi F(q^2)}{\frac{1}{2}\ln[\tau + (1+q^2/\Lambda_{\rm QCD}^2)^2]}, \tag{7}$$

which differs from the MT model in the infrared enhancement term. It ensures the behavior of the effective gluon is in agreement with our modern understanding of QCD's gauge sector; in the minimal Landau gauge in $3+1$ dimensions, the gluon propagator is a bounded, regular function of spacelike momenta and is infrared enhanced [76]. It has been confirmed that the hadron properties are insensitive to small variations of $\omega \in [0.4, 0.6]$, so long as the product $m_G^3 \equiv (\omega D)$ remains constant (typical values of $m_G \sim 0.4$–0.8 GeV) [77,78]. These models have been extensively employed to study hadron physics through the SDEs of QCD, obtaining a wide range of predictions: meson and baryon spectrum and properties [47,79,80], parton distribution amplitudes [77], parton distribution functions [81,82], electromagnetic elastic [83] and transition form factors [84–87], hadronic contribution to the anomalous electromagnetic moment of the muon [88–91], etc.

III. QUARK-GLUON VERTEX

For the 1PI QGV, the simplest choice is to replace the fully dressed fermion-boson vertex by its tree level counterpart. Along with the ladder approximation of the meson Bethe-Salpeter equation, it corresponds to the rainbow-ladder truncation. Even in the Abelian case of QED, this (bare) vertex manages to satisfy the corresponding WGFTI [92–95] only in the chirally symmetric phase in the Landau gauge and in the leading log approximation for the wave-function renormalization [6]. For these particular choices and limits, it ensures $Z(p^2;\mu^2) = 1$ and $M(p^2) = 0$. The simplicity of this choice brings even further undesirable features. It obviously lacks all those six basis structures which are dynamically generated through DCSB. Moreover, the associated dressed quark anomalous chromomagnetic moment and electromagnetic *distribution* in the infrared, associated with DCSB, is much less than what is required from observed hadron phenomenology [96]. Some of these drawbacks can be compensated by a proper choice of parameters in the effective gluon propagator to render good description of pseudoscalar and light vector meson spectra [97]. However, this is not the case with axial vector mesons, since the bare vertex lacks a proper enhancement of the spin-orbit splitting in this channel.

In constructing a fully consistent fermion-boson vertex *Ansatz*, many efforts have been made over the past few decades. We choose to explore [4,5,8,11] for our numerical

investigation. The general form of the vertex consists of 12 linearly independent structures, which can be obtained from three vectors k_μ, p_μ, γ_μ and four spin scalars 1, $\gamma\cdot k$, $\gamma\cdot p$, $\gamma\cdot k\gamma\cdot p$. A first step towards constructing a QGV is employing the STI [30,31]. In addition to the quark propagator, it also involves the ghost propagator and the quark-quark-ghost-ghost scattering kernel. As we work with infrared enhanced effective one gluon exchange models, we can adopt the Abelian approximation of the STI with impunity, namely, the WGFTI which entails

$$iq_\mu\Gamma_\mu = S^{-1}(k) - S^{-1}(p).$$

Following the usual arguments of Ball and Chiu, WGFTI allows this vertex to be decomposed into a longitudinal and a transverse part,

$$\Gamma_\mu(k,p) = \Gamma^L_\mu(k,p) + \Gamma^T_\mu(k,p),$$

such that $q_\mu\Gamma^T_\mu = 0$ and the longitudinal term (Γ^L_μ) is fixed by the above WGFTI. In the so-called Ball-Chiu basis, Γ^L_μ is written as

$$\begin{aligned}\Gamma^{L(BC)}_\mu(k,p) = {}& \lambda_1(k^2,p^2)\gamma_\mu - i\lambda_2(k^2,p^2)t_\mu \\ & + \lambda_3(k^2,p^2)t_\mu\gamma\cdot t/2 + \lambda_4(k^2,p^2)t_\nu\sigma_{\mu\nu},\end{aligned} \tag{8}$$

where the dressing functions are

$$\begin{aligned}\lambda_1(k^2,p^2) &= \bar{\Delta}_A(k^2,p^2),\\ \lambda_2(k^2,p^2) &= \Delta_B(k^2,p^2),\\ \lambda_3(k^2,p^2) &= \Delta_A(k^2,p^2),\\ \lambda_4(k^2,p^2) &= 0,\end{aligned} \tag{9}$$

with $t = k + p$, $(k^2 - p^2)\Delta_\varphi(k^2,p^2) \equiv \varphi(k^2) - \varphi(p^2)$ and $2\bar{\Delta}_\varphi(k^2,p^2) \equiv \varphi(k^2) + \varphi(p^2)$. A generalization of the BC vertex to the non-Abelian case can be found in [19]. Note that although $\lambda_4 = 0$ for QED, the contribution coming from the triple gluon vertex in QCD ensures that it is nonzero for the latter case [41]. However, as we work with the Abelian-ized version of QCD, we will stick to $\lambda_4 = 0$. Notice also that λ_2 carries an explicit dependence on the mass function. It implies that its appearance in the chiral limit owes itself entirely to DCSB. In the following, we will take $\Gamma^L_\mu = \Gamma^{L(BC)}_\mu$ and discuss different choices of Γ^T_μ.

The transverse part is decomposed as a linear combination of the eight basis vectors $T_{i\mu}$, that is

$$\Gamma^T_\mu = \sum_{i=1}^{8}\tau_i(k^2,p^2,q^2)T_{i\mu}(k,p),$$

where τ_i are unknown scalar functions. Rather generally, the basis vectors can be written as

$$\begin{aligned}T_{1\mu}(k,p) &= i[p_\mu(k\cdot q) - k_\mu(p\cdot q)],\\ T_{2\mu}(k,p) &= [p_\mu(k\cdot q) - k_\mu(p\cdot q)]\gamma\cdot t,\\ T_{3\mu}(k,p) &= q^2\gamma_\mu - q_\mu\gamma\cdot q,\\ T_{4\mu}(k,p) &= iq^2[\gamma_\mu\gamma\cdot t - t_\mu] + 2q_\mu p_\nu k_\lambda\sigma_{\nu\lambda},\\ T_{5\mu}(k,p) &= \sigma_{\mu\nu}q_\nu,\\ T_{6\mu}(k,p) &= \gamma_\mu(p^2 - k^2) + t_\mu\gamma\cdot q,\\ T_{7\mu}(k,p) &= \frac{i}{2}(k^2 - p^2)[\gamma_\mu\gamma\cdot t - t_\mu] + t_\mu p_\nu k_\lambda\sigma_{\nu\lambda},\\ T_{8\mu}(k,p) &= -i\gamma_\mu p_\nu k_\lambda\sigma_{\nu\lambda} + k_\mu\gamma\cdot p - p_\mu\gamma\cdot k.\end{aligned} \tag{10}$$

Note that

$$q_\mu T_{i\mu}(k,p) = 0 \qquad i = 1,\ldots,8. \tag{11}$$

This basis is not the one employed in [4]. We choose to work with a modification of this initial basis which was put forward in [98] and later employed in [41] as well. This latter, which we have adopted here, choice ensures all transverse form factors of the vertex are independent of any kinematic singularities in one-loop perturbation theory in an arbitrary covariant gauge.

The determination of the coefficients τ_i is not arbitrary. To a reasonable extent, they are constrained by the TTI, LKFT, MR, freedom of kinematic singularities and the adequate perturbation theory limit in the weak coupling regime [4,9,38].

Curtis and Pennington [5] adopted a simple choice of the transverse coefficients, which ensures MR of the massless electron propagator in the quenched approximation of quantum electrodynamics (QED). This transverse part of the vertex, referred to as the *CP* vertex, is merely

$$\Gamma^{T(CP)}_\mu = \frac{\gamma_\mu(k^2 - p^2) - t_\mu\gamma\cdot t}{2d(k,p)}[A(k^2) - A(p^2)], \tag{12}$$

where $t = k + p$ and

$$d(k,p) = \frac{(k^2 - p^2)^2 + [M^2(k^2) + M^2(p^2)]^2}{k^2 + p^2}.$$

There is a peculiar $[M^2(k^2) + M^2(p^2)]^2$ factor in this *Ansatz*. Notice that its absence introduces an unwanted kinematic singularity. Moreover, it does not jeopardize the MR of the massless electron propagator by construction.

In a subsequent work, Kizilersu and Pennington [11] proposed two vertex constructions for the unquenched case, in the chiral limit with $n_f = 1$. On using any of these two *Ansätze* in the SDEs for the perturbative photon and massless fermion propagators simultaneously, they get the correct power law behavior for the photon dressing function and the fermion wave-function renormalization. Both proposals satisfy the same constraints and differ only

beyond the leading logarithmic order, while also giving similar results in the Landau gauge [11,99]. Thus, one could use either. We choose to work with the following KP construction:

$$\Gamma_\mu^{T(KP)} = \tau_2 T_{2\mu} + \tau_3 T_{3\mu} + \tau_6 T_{6\mu} + \tau_8 T_{8\mu}, \tag{13}$$

where the dressing functions are

$$\begin{aligned}
\tau_2(k^2,p^2,q^2) &= -\frac{4}{3}\frac{1}{k^4-p^4}(A(k^2)-A(p^2)) \\
&\quad -\frac{1}{3}\frac{A(k^2)+A(p^2)}{(k^2+p^2)^2}\ln\left[\frac{A(k^2)A(p^2)}{A(q^2)^2}\right], \\
\tau_3(k^2,p^2,q^2) &= \frac{5}{12}\frac{1}{k^2-p^2}(A(k^2)-A(p^2)) \\
&\quad +\frac{1}{6}\frac{A(k^2)+A(p^2)}{(k^2+p^2)^2}\ln\left[\frac{A(k^2)A(p^2)}{A(q^2)^2}\right], \\
\tau_6(k^2,p^2,q^2) &= -\frac{1}{4}\frac{1}{k^2+p^2}(A(k^2)-A(p^2)), \\
\tau_8(k^2,p^2,q^2) &= 0.
\end{aligned} \tag{14}$$

In 2012, Bashir *et al.* [8] put forward a family of fermion-boson vertices expressed solely in terms of the vector and scalar functions appearing in the fermion propagator. Among other requirements, constraints on a_i ensure the *Ansatz* is consistent with one-loop perturbation theory. For the sake of computational simplicity, the coefficients of the transverse basis are chosen to be independent of the angle between the relative momenta. Strikingly, it also has no explicit dependence on the covariant-gauge parameter. Residual freedom of choice for a_i allows us to achieve the gauge independence of the critical coupling in QED, above which chiral symmetry is dynamically broken. The set of scalar functions τ_i for this proposal is written as

$$\begin{aligned}
\tau_1(k,p) &= \frac{a_1\Delta_B(k^2,p^2)}{(k^2+p^2)}, \\
\tau_2(k,p) &= \frac{a_2\Delta_A(k^2,p^2)}{(k^2+p^2)}, \\
\tau_3(k,p) &= a_3\Delta_A(k^2,p^2), \\
\tau_4(k,p) &= \frac{a_4\Delta_B(k^2,p^2)}{[k^2+M^2(k^2)][p^2+M^2(p^2)]}\frac{k^2-p^2}{4}, \\
\tau_5(k,p) &= +a_5\Delta_B(k^2,p^2), \\
\tau_6(k,p) &= -\frac{a_6(k^4-p^4)\Delta_A(k^2,p^2)}{[(k^2-p^2)^2+(M^2(k^2)+M^2(p^2))^2]}, \\
\tau_7(k,p) &= +\left[\frac{a_7}{(k^2+p^2)}+\frac{2(k-p)^2}{k^2-p^2}\tau_4\right]\Delta_B(k^2,p^2), \\
\tau_8(k,p) &= a_8\Delta_A(k^2,p^2),
\end{aligned} \tag{15}$$

TABLE I. A choice of momentum and gauge-independent coefficients of the transverse basis in the BB fermion-boson vertex [8,9].

Constant	a_1	a_2	a_3	a_4	a_5	a_6	a_7	a_8
Value	0	3.4	1	1	$-4/3$	$-1/2$	2.167	-3.7

where a_i are momentum-independent constants whose values are listed in Table I. Such constants are interconnected by numerous constraints from perturbation theory and gauge covariance. The fixing procedure can be found in Refs. [8,9]. We call this proposal the BB vertex. In the next section we shall discuss the gap equation with all these vertices.

IV. GAP EQUATION

Dressing functions $B(k^2)$ and $A(k^2)$ can be decoupled through proper projections of Eq. (1), viz., multiplying Eq. (1) by $\mathbb{1}$ and $\not{p}$, respectively, and then taking traces.

A. The bare vertex

For this approximation $\Gamma_\mu = \gamma_\mu$, quark self-energy of Eq. (2) acquires the following simple form:

$$\Sigma(p) = Z_1 C_F \int_k g^2 D_{\mu\nu}(q)\gamma_\mu S(k)(Z_2\gamma_\nu). \tag{16}$$

Using the steps suggested above, one arrives at the expressions

$$B(p^2) = m_0 Z_2 + 16\pi Z_2^2 \int_k \frac{\alpha_s(q^2)}{q^2}\sigma_s(k^2), \tag{17}$$

$$\begin{aligned}
A(p^2) &= Z_2 + \frac{16\pi}{3p^2}Z_2^2\int_k \frac{\alpha_s(q^2)}{q^2} \\
&\quad \times \sigma_v(k^2)\left[k\cdot p + \frac{2k\cdot q\, p\cdot q}{q^2}\right].
\end{aligned} \tag{18}$$

This minimal *Ansatz* neglects any non-Abelian contribution to the QGV Therefore, for the sake of consistency, we equate $Z_1 = Z_2$. In fact, we can continue to use it with impunity for the BC, *CP*, KP and BB vertices as they were all proposed in an Abelian setup. Note that this reasoning is no longer valid if the QGV employed is constructed from the corresponding STI because this extended identity incorporates the effects coming from the non-Abelian ghost-gluon sector. However, note that the renormalization boundary condition, independently of the truncation, entails

$$S^{-1}(p)|_{p^2=\mu^2} = i\gamma\cdot p + m(\mu),$$

where $m(\mu) = M(\mu^2)$ is the scale dependent running quark mass. The above condition implies $A(p^2=\mu^2) = 1$ and

$B(p^2=\mu^2)=m(\mu)$. One can thus define a convenient renormalization point invariant mass as follows:

$$\hat{m}=m(\mu)\left[\frac{1}{2}\ln\left(\frac{\mu^2}{\Lambda^2_{\rm QCD}}\right)\right]^{\gamma_m}. \tag{19}$$

B. The BC vertex

Returning to the gap equation and the QGV, if one employs the BC vertex, Eq. (17) modifies as

$$B(p^2)=m_0Z_2+\frac{16\pi}{3}Z_2\int_k\frac{\alpha_s(q^2)}{q^2}\times\{\sigma_s(k^2)[I^{BC}_{B1}+I^{BC}_{B2}]+\sigma_v(k^2)[I^{BC}_{B3}]\}, \tag{20}$$

where I^{BC}_{B1}, I^{BC}_{B2} and I^{BC}_{B3} are the integrands related to the BC vertex, such that

$$I^{BC}_{B1}=3\frac{A(k^2)+A(p^2)}{2},$$
$$I^{BC}_{B2}=\Delta_A(k^2,p^2)\left\{\frac{t^2q^2-(t\cdot q)^2}{2q^2}\right\},$$
$$I^{BC}_{B3}=\Delta_B(k^2,p^2)\left\{\frac{q^2t\cdot k-t\cdot qq\cdot k}{q^2}\right\}.$$

Analogously, the corresponding equation for $A(p^2)$ is

$$A(p^2)=Z_2+\frac{16\pi}{3}Z_2\int_k\frac{\alpha_s(q^2)}{q^2}\times\{\sigma_v(k^2)[I^{BC}_{A1}-I^{BC}_{A2}]+\sigma_s(k^2)[I^{BC}_{A3}]\}, \tag{21}$$

where the integrands are written as

$$I^{BC}_{A1}=\frac{A(k^2)+A(p^2)}{2}\frac{1}{p^2}\times\left\{\frac{k\cdot pq^2+2[(k^2+p^2)k\cdot p-k^2p^2-k\cdot p^2]}{q^2}\right\},$$
$$I^{BC}_{A2}=\frac{1}{2p^2}\Delta_A(k^2,p^2)\times\left\{[p^2k+k^2p]\cdot t-\frac{p^2t\cdot qk\cdot q-k^2t\cdot qp\cdot q}{q^2}\right\},$$
$$I^{BC}_{A3}=\Delta_B(k^2,p^2)\frac{1}{p^2}\left\{\frac{t\cdot qp\cdot q-t\cdot pq^2}{q^2}\right\}.$$

C. The *CP* vertex

By taking into account the transverse CP vertex, one arrives at

$$B(p^2)=m_0Z_2+\frac{16\pi}{3}Z_2\int_k\frac{\alpha_s(q^2)}{q^2}\times\left\{\sigma_s(k^2)[I^{BC}_{B1}+I^{BC}_{B2}]+\sigma_v(k^2)[I^{BC}_{B3}]+\frac{3}{2}\sigma_s(k^2)(k^2+p^2)L(k^2+p^2)\right\}, \tag{22}$$

where $L\equiv L(k^2,p^2)$ is defined as

$$L=\frac{[A^2(k^2)A^2(p^2)]^2\Delta_A(k^2,p^2)}{[A^2(k^2)A^2(p^2)]^2+[A^2(p^2)B^2(k^2)+A^2(k^2)B^2(p^2)]^2}.$$

On the other hand, the analogous expression for $A(p^2)$ reads as

$$A(p^2)=Z_2+\frac{16\pi}{3}Z_2\int_k\frac{\alpha_s(q^2)}{q^2}\times\left\{\sigma_v(k^2)[I^{BC}_{A1}-I^{BC}_{A2}]+\sigma_s(k^2)[I^{BC}_{A3}]+2\sigma_v(k^2)\frac{k^2+p^2}{k^2-p^2}[I^{CP}_{A1}+I^{CP}_{A2}]L(k^2,p^2)\right\}. \tag{23}$$

The integrands I^{CP}_{A1} and I^{CP}_{A2}, related to the CP term, are

$$I^{CP}_{A1}=(k^2-p^2)\left\{\frac{3(k^2+p^2)k\cdot p-2k^2p^2-4k\cdot p^2}{q^2}\right\},$$
$$I^{CP}_{A2}=k^2t\cdot p-p^2t\cdot k+\frac{p^2t\cdot qk\cdot q-k^2t\cdot qp\cdot q}{q^2}.$$

D. The KP vertex

The KP vertex *Ansatz* yields the following equation for $B(p^2)$:

$$B(p^2)=m_0Z_2+\frac{16\pi}{3}Z_2\int_k\frac{\alpha_s(q^2)}{q^2}\times\{\sigma_s(k^2)[I^{BC}_{B1}+I^{BC}_{B2}]+\sigma_v(k^2)[I^{BC}_{B3}]+\sigma_s(k^2)[I^{KP}_{B1}-I^{KP}_{B2}-I^{KP}_{B3}]\}. \tag{24}$$

The integrands related specifically to the KP vertex, I^{KP}_{B1}, I^{KP}_{B2} and I^{KP}_{B3}, can be expressed as

$$I^{KP}_{B1} = 2(k\cdot p^2 - k^2 p^2)\left\{\frac{4}{3}\frac{A(k^2)-A(p^2)}{k^4-p^4} + \frac{1}{3}\frac{A(k^2)+A(p^2)}{(k^2+p^2)^2}\ln\left[\frac{A(k^2)A(p^2)}{A^2(q^2)}\right]\right\},$$
$$I^{KP}_{B2} = q^2\left\{\frac{5}{4}\Delta_A(k^2,p^2), + \frac{1}{2}\frac{A(k^2)+A(p^2)}{k^2+p^2}\ln\left[\frac{A(k^2)A(p^2)}{A^2(q^2)}\right]\right\},$$
$$I^{KP}_{B3} = \frac{3}{4}(k^2-p^2)\frac{A(k^2)-A(p^2)}{k^2+p^2}.$$

The corresponding equation for $A(p^2)$, for KP vertex, is

$$A(p^2) = Z_2 + Z_2\frac{16\pi}{3}\int_k \frac{\alpha_s(q^2)}{q^2}\{\sigma_v(k^2)[I^{BC}_{A1} - I^{BC}_{A2}] + \sigma_s(k^2)[I^{BC}_{A3}] + \sigma_v(k^2)(I^{KP}_{A1} + I^{KP}_{A2} - I^{KP}_{A3})\}, \tag{25}$$

where the related integrands are

$$I^{KP}_{A1} = \frac{(k^2+p^2)(k^2p^2 - k.p^2)}{p^2}\left\{\frac{4}{3}\frac{A(k^2)-A(p^2)}{k^4-p^4} + \frac{1}{3}\frac{A(k^2)+A(p^2)}{(k^2+p^2)^2}\ln\left[\frac{A(k^2)A(p^2)}{A^2(q^2)}\right]\right\},$$
$$I^{KP}_{A2} = \frac{k\cdot p(4k\cdot p - 3p^2) + k^2(2p^2 - 3k\cdot p)}{p^2}\left\{\frac{5}{12}\Delta_A(k^2,p^2) + \frac{1}{6}\frac{A(k^2)+A(p^2)}{k^2+p^2}\ln\left[\frac{A(k^2)A(p^2)}{A^2(q^2)}\right]\right\},$$
$$I^{KP}_{A3} = \frac{3}{4}A(k^2)[A(k^2)-A(p^2)]\frac{(k^2-p^2)}{(k^2+p^2)}\frac{k\cdot p}{p^2}.$$

Unlike the other vertex *Ansätze*, the transverse part of the KP vertex introduces a nontrivial angular dependence, in connection to the logarithmic terms which contain $A(q^2)$. Thus, the numerical evaluation of such integrals is considerably more complicated.

E. The BB vertex

Finally, the integral equations for the scalar functions $B(p^2)$ and $A(p^2)$, using the BB vertex [8] are written as

$$\begin{aligned} B(p^2) = {} & \text{rhs of Eq. (20)} - \frac{16\pi}{3}Z_2\int_k \frac{\alpha_s(q^2)}{q^2}\frac{1}{k^2A^2(k^2)+B^2(k^2)}\Big\{A(k^2)((k\cdot p)^2 - k^2p^2)\tau_1 \\ & + 2B(k^2)((k\cdot p)^2 - k^2p^2)\tau_2 - 3B(k^2)(k^2+p^2-2k\cdot p)\tau_3 + A(k^2)[k^2(p^2-3k\cdot p) \\ & + k\cdot p(3p^2 - 4k\cdot p) + 3k^4]\tau_4 + 3A(k^2)(k^2 - k\cdot p)\tau_5 + 3B(k^2)(k^2-p^2)\tau_6 \\ & + \frac{A(k^2)}{2}[k^2(3k\cdot p - p^2) - k\cdot p(2k\cdot p + 3p^2) + 3k^4)]\tau_7 \\ & + 3a_8B(k^2)k\cdot p\Delta_A(k^2,p^2)\Big\}, \end{aligned} \tag{26}$$

$$\begin{aligned} A(p^2) = {} & \text{rhs of Eq. 21} - \frac{16\pi}{3}Z_2\int_k \frac{\alpha_s(q^2)}{q^2}\frac{1}{k^2A^2(k^2)+B^2(k^2)}\frac{1}{p^2}\Big\{B(k^2)((k\cdot p)^2 - k^2p^2)\tau_1 + A(k^2)(k^2(p^4 - (k\cdot p)^2) \\ & - p^2(k\cdot p)^2 + k^4p^2)\tau_2 - A(k^2)(k^2(3k\cdot p - 2p^2) + k\cdot p(3p^2 - 4k\cdot p))\tau_3 - B(k^2)[-4(k\cdot p)^2 - 3p^2(k\cdot p) \\ & + k^2(3k\cdot p + p^2) + 3p^4]\tau_4 + 3B(k^2)(p^2 - k\cdot p)\tau_5 + 3A(k^2)(k^2-p^2)(k\cdot p)\tau_6 \\ & - \frac{B(k^2)}{2}[2(k\cdot p)^2 - 3p^2(k\cdot p) + k^2(3k\cdot p + p^2) - 3p^4]\tau_7 - 2A(k^2)((k\cdot p)^2 - k^2p^2)\tau_8\Big\}. \end{aligned} \tag{27}$$

In the next section, we present and discuss the numerical results obtained from employing different vertex *Ansätze* we chose to study the gap equation with.

V. RESULTS

We solve the gap equation for a few largely employed quark-gluon vertices suggested in literature over the past three decades. This exercise is carried out in conjunction with effective MT and QC models for the gluon propagator. The renormalization point is set to $\mu \equiv \mu_3 = 2.86$ GeV. The infrared strength of the gluon models is fixed from the chiral quark condensate [100], as we now explain. Note that the chiral limit is defined when $\hat{m} = 0$ ($\mu \to \infty$) in Eq. (19) and we label it as m_q. In this limit, we can express the chiral quark condensate as follows:

$$-\langle\bar{q}q\rangle^0_\mu = Z_4 N_c \mathrm{Tr} \int_k S_{\hat{m}}(k;\mu). \tag{28}$$

We can thus define a renormalization point invariant condensate $\langle\bar{q}q\rangle$ as

$$m(\mu)\langle\bar{q}q\rangle^0_\mu = \hat{m}\langle\bar{q}q\rangle. \tag{29}$$

It is an order parameter of DCSB and, as explained elsewhere [101,102], it is also the chiral limit value of the in-meson condensate. Therefore, it is natural to fix the effective gluon strength to produce a reasonable value of the chiral quark condensate and study its impact on other quantities. We fix MT and QC gluon model parameters, ω and the product ωD, to obtain $-\langle\bar{q}q\rangle^0_{\mu_3} = (0.256\ \mathrm{GeV})^3$. Along with Eq. (29), this value yields $-\langle\bar{q}q\rangle^0_{\mu_2} = (0.250\ \mathrm{GeV})^3$ and $-\langle\bar{q}q\rangle^0_{\mu_{19}} = (0.280\ \mathrm{GeV})^3$ (where $\mu_{2,19} =$ 2, 19 GeV), in agreement with modern estimates [87]. The specific choice of parameters is displayed in Table II. The resulting chiral limit mass functions are shown in Figs. 2 and 3, along with those obtained for different nonzero current quark masses: $m(\mu) = 0.004$, 0.1, 1.0, 4.1 GeV, labeled as $m_{u/d}, m_s, m_c$ and m_b, respectively (the $m_{u/d}$ results are not displayed, in order to avoid overlap with the chiral limit results). In an intermediate range of momenta, Figs. 4 and 5 show a more pronounced comparison of chiral limit results for different *Ansätze* of the QGV.

The mass functions exhibit the expected features; namely, saturation at a finite value as $p^2 \to 0$ and a monotonic decrease as p^2 increases. The saturation value, $M(0)$, in comparison with the current quark mass, is expectedly much larger in the case of the light quarks and it decreases sharply with increasing p^2, whereas it exhibits far less steep running for the heavy quarks. It is clear that dynamical mass generation via strong-interaction processes (DCSB) is the dominant mass generating mechanism in the light sector, while the heavy sector is largely overshadowed by its predominant coupling to the Higgs field.

Also readily observed is the fact that bare vertex calculations tend to produce larger values of $M(0)$ [although the asymptotic behavior of $M(p^2)$ for $p^2 \to \infty$ is reached faster]. This is a consequence of the artificial enhancement of the effective coupling in order to produce a sufficient

TABLE II. Gluon model parameters ω and $m_G = (\omega D)^{1/3}$ for each vertex *Ansatz*. Dimensioned quantities are expressed in GeV.

Vertex	ω	m_G	ω	m_G
	MT model [50]		QC model [28]	
Bare	0.4	0.728	0.4	0.744
BC [4]	0.4	0.528	0.48	0.583
CP [5]	0.4	0.516	0.4	0.529
KP [11]	0.4	0.528	0.46	0.551
BB [8]	0.4	0.544	0.4	0.562

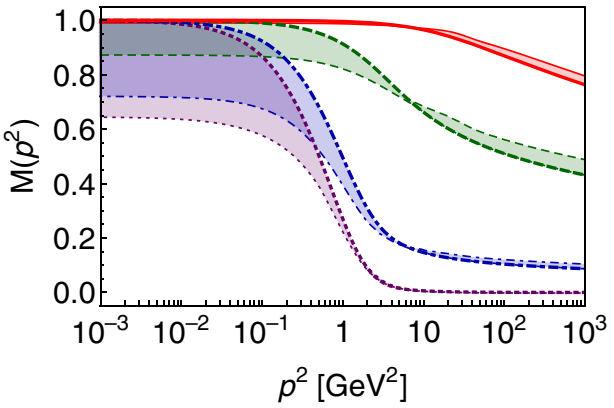

FIG. 2. (MT model) Mass functions for different current quark masses and QGV *Ansätze*. The boundaries of the bands are given by the lowest and highest produced values of $M(p^2)$, for the different vertices: BC, *CP*, KP, BB and the bare vertex. The purple band with dotted boundaries corresponds to the chiral limit. Blue (dot dashed boundary), green (dashed boundary) and red (solid boundary) bands correspond to $m_s = 0.1$ GeV, $m_c = 1$ GeV and $m_b = 4.1$ GeV, respectively. Mass functions or each quark flavor have been normalized such that $M_{\max}(0) = 1$. Bare vertex results are highlighted with a thicker line which forms the top edge of each band.

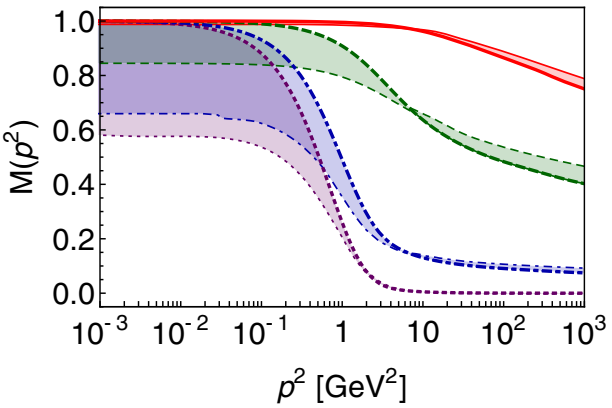

FIG. 3. (QC model) Mass functions for different current quark masses and QGV *Ansätze*. Bands and curves have the same meaning as in Fig. 2.

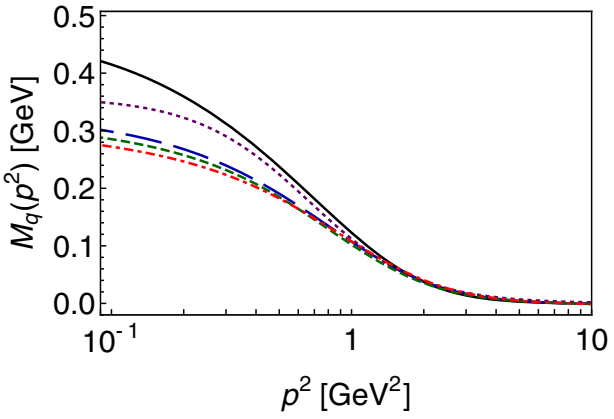

FIG. 4. (MT model) Chiral limit mass functions from different QGV *Ansätze*. Bare (black, solid), Ball-Chiu (blue, long dashed), Curtis-Pennington (green, dashed), Kizilerzu-Pennington (Red, dot dashed) and Bashir-Bermudez (purple, dotted) vertex *Ansätze*.

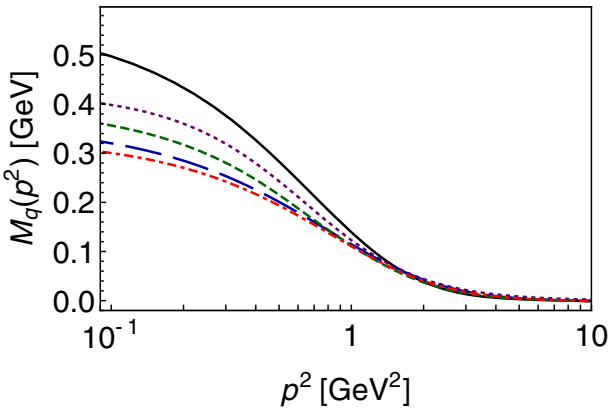

FIG. 5. (QC model) Chiral limit mass functions from different QGV *Ansätze*. Curves are labeled as in Fig. 4.

amount of phenomenologically required DCSB.[1] In fact, if the infrared gluon model were enhanced just as much as with the other vertices, chiral condensate and $M(0)$ would decrease 40%–60%. Moreover, had we omitted the bare vertex results, the bands in Figs. 2 and 3 would have become much narrower. This is exactly what is displayed in Figs. 6 and 7. It clearly indicates that the results obtained from properly constructed quark-gluon vertices are more robust and less sensitive to the gluon model parameters.

Another important feature of the mass function is its asymptotic behavior. In the chiral limit [100,103],

$$M(p^2 \to \infty) \sim \frac{\ln\left[p^2/\Lambda_{\rm QCD}^2\right]^{\gamma_m - 1}}{p^2}. \tag{30}$$

[1]It provides the strength needed to simultaneously produce reasonable values of vacuum quark condensate, mass spectrum and decay constants.

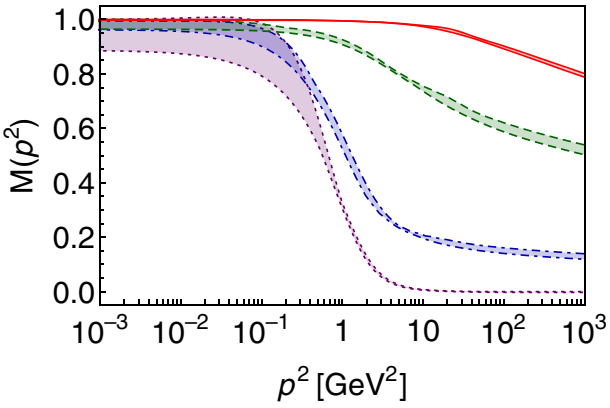

FIG. 6. (MT model) Mass functions for different current quark masses and QGV *Ansätze*. Bands and curves have the same meaning as in Fig. 2. However, the bare vertex results have been omitted in this figure.

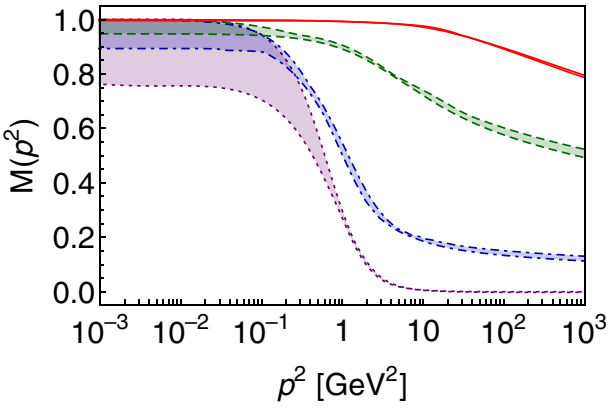

FIG. 7. (QC model) Mass functions for different current quark masses and QGV *Ansätze*. Bands and curves have the same meaning as in Fig. 2. The bare vertex results have again been excluded to bring out the robustness of the results for the dressed vertices.

Naturally, since bare vertex is the leading order term in the perturbative expansion, mass function reaches this behavior faster in such case. It is followed (consistently with both MT and QC interactions) by *CP*, BC, KP and BB vertices, respectively. Beyond the chiral limit, Eq. (30) is modified by including an extra term, which is proportional to the current quark mass [100,103], but the overall pattern persists.

To further understand the interplay between explicit and dynamical mass generation, let us define the following quantity:

$$\bar{M}(m) = \left|\frac{M_E - m(\mu)}{M_E}\right|, \tag{31}$$

where M_E, the constituent Euclidian mass, is defined through

$$M_E^2 \equiv \{p^2 | p^2 = M^2(p^2)\}.$$

TABLE III. Calculated constituent quark masses $M(0)$ for different current quark masses and QGV *Ansätze*. Dimensioned quantities are expressed in GeV. Gluon model parameters are shown in Table II.

Vertex	m_q	$m_{u/d}$	m_s	m_c	m_b
		MT model [50]			
Bare	0.484	0.492	0.649	1.464	4.228
BC [4]	0.331	0.337	0.468	1.284	4.186
CP [5]	0.315	0.323	0.468	1.279	4.184
KP [11]	0.306	0.315	0.471	1.297	4.186
BB [8]	0.353	0.356	0.483	1.186	4.072
		QC model [28]			
Bare	0.573	0.581	0.730	1.520	4.240
BC [4]	0.360	0.366	0.485	1.295	4.188
CP [5]	0.399	0.403	0.502	1.284	4.185
KP [11]	0.330	0.339	0.479	1.296	4.187
BB [8]	0.435	0.438	0.512	1.186	4.055

Naturally, $\bar{M}(m) \to 1$ as $m(\mu) \to 0$, while $\bar{M}(m)$ smoothly approaches zero with increasing current quark mass, as the explicit mass generation becomes dominant. Therefore, one can interpret the vicinity around $m_{\rm crit}$, $m_{\rm crit} \equiv \{m(\mu)|\bar{M}(m) = 1/2\}$, as the region in which the strengths of explicit and dynamical chiral symmetry breaking are comparable. We find that $m_{\rm crit} \approx 0.284$ GeV, consistent with that obtained in [104], from different criteria. Notice that $m_{\rm crit}$ lies between charm and strange quark masses, but closer to the latter; thus, strange quark can be considered as the boundary between the strong and weak mass generation mechanism being dominant [87]. Explicit values of $M(0)$ and M_E for a set of current quark masses $(m_q, m_{u/d}, m_s, m_c, m_b)$ are listed in Tables III and IV. Figure 8 shows $\bar{M}(m)$ in a range of values of $m(\mu)$. Notably, $\bar{M}(m)$ is practically insensitive to the choice of the fully dressed QGV (and gluon models), while those obtained from the bare vertex lie closely. Our observations are thus practically model independent statements.

TABLE IV. Calculated Euclidean constituent quark masses M_E for different current quark masses and QGV *Ansätze*. Dimensioned quantities are expressed in GeV. Gluon model parameters are shown in Table II.

Vertex	m_q	$m_{u/d}$	m_s	m_c	m_b
		MT model [50]			
Bare	0.388	0.395	0.523	1.274	4.016
BC [4]	0.301	0.307	0.417	1.184	4.037
CP [5]	0.290	0.297	0.419	1.181	4.038
KP [11]	0.280	0.287	0.430	1.198	4.036
BB [8]	0.344	0.347	0.445	1.186	4.072
		QC model [50]			
Bare	0.442	0.449	0.574	1.303	4.009
BC [4]	0.319	0.324	0.429	1.191	4.036
CP [5]	0.347	0.352	0.439	1.183	4.038
KP [11]	0.302	0.310	0.435	1.199	4.036
BB [8]	0.390	0.391	0.449	1.173	4.055

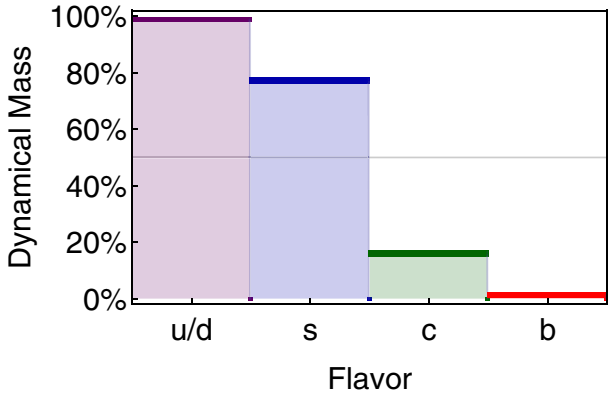

FIG. 8. Dynamical versus explicit mass generation as defined in Eq. (31). The narrow darker regions correspond to the uncertainty coming from the choice of the QGV (BC, *CP*, KP, BB) and effective coupling (MT or QC). The horizontal line at the 50% mark corresponds to $m(\mu) = m_{\rm crit} \approx 0.284$ GeV. It lies between the strange and charm quark masses. It corresponds to the ratio of dynamical vs explicit mass generation being $\bar{M}(m) = 1/2$.

Another interesting measure of DCSB is given by the pseudoscalar meson leptonic decay constant, f_π. The chiral limit value can be easily computed from [103]:

$$f_\pi^2 = \frac{3}{4\pi^2}\int dp^2 \frac{p^2 Z(p^2) M(p^2)}{[p^2 + M^2(p^2)]^2}\left[M(p^2) - \frac{p^2}{2}M'(p^2)\right] \tag{32}$$

and from the improved Pagels-Stokar-Cornwall formula derived in [105]:

$$f_\pi^2 = \frac{3}{8\pi^2}\int dp^2 p^2 B^2(p^2)(\sigma_v^2 - 2[\sigma_s\sigma_s' + p^2\sigma_v\sigma_v'] - p^2[\sigma_s\sigma_s'' - \sigma_s'\sigma_s'] - p^4[\sigma_v\sigma_v'' - \sigma_v'\sigma_v']), \tag{33}$$

where the dependence of $\sigma_{s,v}$ on p^2 has been omitted for notational convenience. We denote Eqs. (32) and (33) as F.1 and F.2, respectively. The obtained values are shown in Table V. Unsurprisingly, for all dressed vertices employed

TABLE V. Chiral limit decay constants computed from Eqs. (32) and (33) (F.1 and F.2, respectively). Dimensioned quantities are expressed in GeV.

Vertex	F.1	F.2	F.1	F.2
	MT model [50]		QC model [28]	
Bare	0.088	0.101	0.088	0.106
BC [4]	0.083	0.093	0.079	0.093
CP [5]	0.082	0.091	0.082	0.094
KP [11]	0.080	0.090	0.078	0.090
BB [8]	0.085	0.100	0.088	0.103

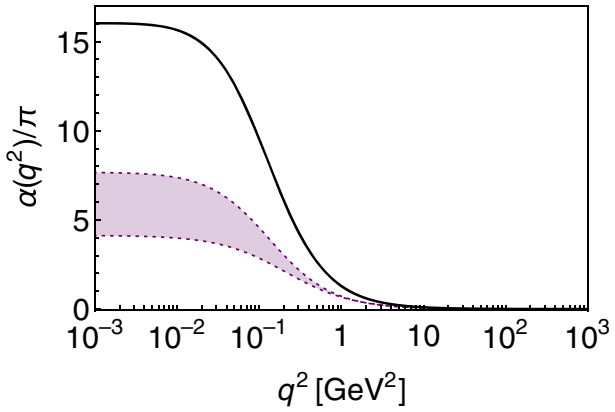

FIG. 9. (QC model) Effective coupling parametrized as in Eq. (34). The black line corresponds to the effective coupling associated with the bare vertex. Results for the other vertices lie within the band whose height is considerably diminished.

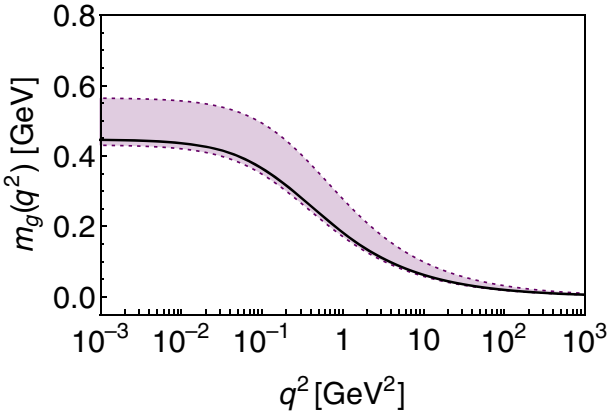

FIG. 10. (QC model) The gluon *running mass* from Eq. (34). The black line corresponds to the effective coupling associated with the bare vertex. Results for the other vertices lie within the band.

herein, F.2 provides a better estimate of the chiral limit value of f_π (≈0.09 GeV). For the BB vertex, both formulas produce very similar values (with a relative difference of ∼2%–4%), while those obtained with BC and KP differ up to 12%–16%. In general, as can be inferred from Tables III to V, BB vertex results exhibit less sensitivity to the choice of MT or QC interaction models. If the bare vertex is employed instead, F.1 gives better estimates than the *more accurate* F.2, which overestimates f_π by 12%–14%. In analogy to the relative largeness of $M(0)$ of the light quarks (of the bare vertex results with respect to the others), this feature could arise from the fact that the rainbow approximation requires larger infrared enhancement from the gluon model. To address this fact, we rewrite QC interaction as follows:

$$\frac{\alpha_s(q^2)}{q^2} \to \frac{\tilde{\alpha}_s(q^2)}{q^2 + m_g^2(q^2)}, \qquad m_g^2(q^2) = \frac{m_0^4}{q^2 + m_0^2}, \tag{34}$$

where $\tilde{\alpha}_s(q^2)$ is parametrized as suggested in the combined SDE and lattice study [106] such that $m_g(q^2)$ acts as a running-mass-like term and provides us with a *gluon mass scale*. Figure 9 clearly shows that a considerable enhancement of the coupling $\alpha(0)/\pi$ is needed for the bare vertex. It is 3.5–5.5 times larger than the corresponding values of the coupling for the other vertices to produce observed phenomenology. Note that it is despite the fact that $m_g(0)$ lies within a typical range ≈0.4–0.6 GeV in all cases, Fig. 10.

Finally, motivated by the GellMann-Oakes-Renner relationship (see [102], for example) and our values of chiral condensate and decay constants, one could argue that m_π can be accurately obtained from realistic solutions of the Bethe-Salpeter equation, with a fully-consistent symmetry-preserving kernel. This is an outstanding challenge that we shall address elsewhere.

VI. CONCLUSIONS AND SCOPE

We have investigated the features of the dressed QGV and their impact on DCSB through the SDE for the quark propagator. Within a small phenomenologically sensible variation of the MT and QC model parameters, fixed solely by the chiral quark condensate, the results obtained from the refined vertex *Ansätze* exhibit very similar quantitative behavior. The robustness of the momentum-dependent mass function and the pion decay constant suggests that hadron observables could be accurately reproduced. Though the bare vertex results for the condensate and the decay constant compare well with other truncations, a notorious infrared enhancement (in the gluon models) is required. First, recall that half of the structures which define the QGV can only contribute if chiral symmetry is dynamically broken. Second, there is a natural interplay between the role of the gluon propagator and the QGV. In order to generate required amount of DCSB, the bare vertex result depends on large infrared enhancement of the gluon propagator as it receives no such contribution from the dynamically generated vertex structures which are left out in this truncation scheme. A realistic and currently converging understanding of the gluon propagator can generate an acceptable running quark mass, via QCD's gap equation, only as long as the QGV exhibits material infrared enhancement itself. Thus an intimate connection between the QGV and the DCSB is established. In this article, employing the MT and QC gluon models, we solve the gap equation using the following vertex *Ansätze*: bare, BC, *CP*, KP and BB. All truncations described herein point towards the same qualitative pattern of DCSB. Expectedly, apart from the bare vertex, the infrared enhancement band of the mass function for all the other *Ansätze* is rather narrow. Its width is what we expect to introduce error bars when we predict hadron observables using this formalism.

The light quarks, weakly coupled to the Higgs field, owe their mass primarily to the infrared QCD dynamics. As one moves towards the heavy sector, weak mass generation commensurates with that coming from QCD's strong interactions; it is between the strange and charm quark masses (but closer to the former) that emergent and explicit mass generation have equal strength. These are qualitatively robust features of the SDE studies [87,104], independent of the details of the truncation.

To enhance the connection with hadron physics, it would be worth investigating if the vertex *Ansätze* studied in this work are suitable for use in the nonperturbative studies of sophisticated hadron physics phenomenology in its fine details, the electromagnetic and transition form factors.

An immediate task would be writing a consistent Bethe-Salpeter kernel for all those vertices. It is known that, along with the bare QGV, a ladder-like kernel is sufficient for many needs, providing an accurate description of light pseudoscalars and vector mesons (see for example, [77,84,86,107]). Nevertheless, for a fully-dressed QGV, the construction of a consistent Bethe-Salpeter kernel could be the next challenge [27,29]. Moreover, DCSB generates a momentum-dependent dressed-quark anomalous chromomagnetic moment, which is large at infrared momenta and has an impact on the mass splitting between parity partners [8,96,108]. Thus, we strongly believe that the truncations which go beyond RL should be relevant for a variety of hadron properties, including the spectrum of the excited states, and the nucleon electromagnetic elastic and transition form factors such as [47,48,109,110]. Some of those aspects are currently being investigated and will be reported elsewhere.

ACKNOWLEDGMENTS

This research was partly supported by *Coordinación de la Investigación Científica* (CIC) of the University of Michoacan and CONACyT-Mexico through Grants No. 4.10 and No. CB2014-22117, respectively. K. R. acknowledges support from CONACyT-Mexico. F. A. acknowledges the financial support of HEC of Pakistan through Project No. 20-4500/NRPU/R&D/HEC/14/727.

[1] J. S. Schwinger, On the Green's functions of quantized fields. 1, Proc. Natl. Acad. Sci. U.S.A. **37**, 452 (1951).
[2] J. S. Schwinger, On the Green's functions of quantized fields. 2, Proc. Natl. Acad. Sci. U.S.A. **37**, 455 (1951).
[3] F. J. Dyson, The S matrix in quantum electrodynamics, Phys. Rev. **75**, 1736 (1949).
[4] J. S. Ball and T.-W. Chiu, Analytic properties of the vertex function in gauge theories. 1, Phys. Rev. D **22**, 2542 (1980).
[5] D. C. Curtis and M. R. Pennington, Truncating the Schwinger-Dyson equations: How multiplicative renormalizability and the Ward identity restrict the three-point vertex in QED, Phys. Rev. D **42**, 4165 (1990).
[6] A. Bashir and M. R. Pennington, Gauge independent chiral symmetry breaking in quenched QED, Phys. Rev. D **50**, 7679 (1994).
[7] A. Bashir and M. R. Pennington, Constraint on the QED vertex from the mass anomalous dimension gamma$(m) = 1$, Phys. Rev. D **53**, 4694 (1996).
[8] A. Bashir, R. Bermudez, L. Chang, and C. D. Roberts, Dynamical chiral symmetry breaking and the fermion–gauge-boson vertex, Phys. Rev. C **85**, 045205 (2012).
[9] L. Albino, A. Bashir, L. X. Gutiérrez Guerrero, B. El Bennich, and E. Rojas, Transverse Takahashi identities and their implications for gauge independent dynamical chiral symmetry breaking, Phys. Rev. D **100**, 054028 (2019).
[10] R. Alkofer, C. S. Fischer, and R. Williams, U(A)(1) anomaly and eta-prime mass from an infrared singular quark-gluon vertex, Eur. Phys. J. A **38**, 53 (2008).
[11] A. Kizilersu and M. R. Pennington, Building the full fermion-photon vertex of QED by imposing multiplicative renormalizability of the Schwinger-Dyson equations for the fermion and photon propagators, Phys. Rev. D **79**, 125020 (2009).
[12] E. Rojas, J. P. B. C. de Melo, B. El-Bennich, O. Oliveira, and T. Frederico, On the quark-gluon vertex and quark-ghost kernel: Combining lattice simulations with Dyson-Schwinger equations, J. High Energy Phys. 10 (2013) 193.
[13] A. C. Aguilar, D. Binosi, D. Ibañez, and J. Papavassiliou, New method for determining the quark-gluon vertex, Phys. Rev. D **90**, 065027 (2014).
[14] R. Williams, The quark-gluon vertex in Landau gauge bound-state studies, Eur. Phys. J. A **51**, 57 (2015).
[15] M. Gomez-Rocha, T. Hilger, and A. Krassnigg, Effects of a dressed quark-gluon vertex in pseudoscalar heavy-light mesons, Phys. Rev. D **92**, 054030 (2015).
[16] M. Gómez-Rocha, T. Hilger, and A. Krassnigg, Effects of a dressed quark-gluon vertex in vector heavy-light mesons and theory average of the B_c^* meson mass, Phys. Rev. D **93**, 074010 (2016).
[17] D. Binosi, L. Chang, J. Papavassiliou, S.-X. Qin, and C. D. Roberts, Natural constraints on the gluon-quark vertex, Phys. Rev. D **95**, 031501 (2017).
[18] R. Bermudez, L. Albino, L. X. Gutiérrez-Guerrero, M. E. Tejeda-Yeomans, and A. Bashir, Quark-gluon vertex: A perturbation theory primer and beyond, Phys. Rev. D **95**, 034041 (2017).
[19] A. C. Aguilar, J. C. Cardona, M. N. Ferreira, and J. Papavassiliou, Quark gap equation with non-Abelian Ball-Chiu vertex, Phys. Rev. D **98**, 014002 (2018).
[20] C. S. Fischer, Infrared properties of QCD from Dyson-Schwinger equations, J. Phys. G **32**, R253 (2006).

[21] R. Alkofer, C. S. Fischer, F. J. Llanes-Estrada, and K. Schwenzer, The quark-gluon vertex in Landau gauge QCD: Its role in dynamical chiral symmetry breaking and quark confinement, Ann. Phys. (Amsterdam) **324**, 106 (2009).

[22] A. Bashir, L. Chang, I. C. Cloet, B. El-Bennich, Y.-X. Liu, C. D. Roberts, and P. C. Tandy, Collective perspective on advances in Dyson-Schwinger equation QCD, Commun. Theor. Phys. **58**, 79 (2012).

[23] I. G. Aznauryan *et al.*, Studies of nucleon resonance structure in exclusive meson electroproduction, Int. J. Mod. Phys. E **22**, 1330015 (2013).

[24] I. C. Cloet and C. D. Roberts, Explanation and prediction of observables using continuum strong QCD, Prog. Part. Nucl. Phys. **77**, 1 (2014).

[25] T. Horn and C. D. Roberts, The pion: An enigma within the standard model, J. Phys. G **43**, 073001 (2016).

[26] C. D. Roberts, Empirical consequences of emergent mass, Symmetry **12**, 1468 (2020).

[27] L. Chang and C. D. Roberts, Sketching the Bethe-Salpeter Kernel, Phys. Rev. Lett. **103**, 081601 (2009).

[28] S.-x. Qin, L. Chang, Y.-x. Liu, C. D. Roberts, and D. J. Wilson, Interaction model for the gap equation, Phys. Rev. C **84**, 042202 (2011).

[29] D. Binosi, L. Chang, J. Papavassiliou, S.-X. Qin, and C. D. Roberts, Symmetry preserving truncations of the gap and Bethe-Salpeter equations, Phys. Rev. D **93**, 096010 (2016).

[30] A. A. Slavnov, Ward identities in gauge theories, Teor. Mat. Fiz. **10**, 153 (1972) [Theor. Math. Phys. **10**, 99 (1972)].

[31] J. C. Taylor, Ward identities and charge renormalization of the Yang-Mills field, Nucl. Phys. **B33**, 436 (1971).

[32] M. J. Aslam, A. Bashir, and L. X. Gutierrez-Guerrero, Local gauge transformation for the quark propagator in an SU(N) gauge theory, Phys. Rev. D **93**, 076001 (2016).

[33] T. De Meerleer, D. Dudal, S. P. Sorella, P. Dall'Olio, and A. Bashir, Fresh look at the Abelian and non-Abelian Landau-Khalatnikov-Fradkin transformations, Phys. Rev. D **97**, 074017 (2018).

[34] T. De Meerleer, D. Dudal, S. P. Sorella, P. Dall'Olio, and A. Bashir, Landau-Khalatnikov-Fradkin transformations, Nielsen identities, their equivalence and implications for QCD, Phys. Rev. D **101**, 085005 (2020).

[35] Y. Takahashi, in *Canonical Quantization and Generalized Ward Relations: Foundation of Nonperturbative Approach* (Positano Symp., 1985), p. 0019.

[36] K.-I. Kondo, Transverse Ward-Takahashi identity, anomaly and Schwinger-Dyson equation, Int. J. Mod. Phys. A **12**, 5651 (1997).

[37] H.-X. He, F. C. Khanna, and Y. Takahashi, Transverse Ward-Takahashi identity for the fermion boson vertex in gauge theories, Phys. Lett. B **480**, 222 (2000).

[38] S.-X. Qin, L. Chang, Y.-X. Liu, C. D. Roberts, and S. M. Schmidt, Practical corollaries of transverse Ward-Green-Takahashi identities, Phys. Lett. B **722**, 384 (2013).

[39] Y.-D. Li and Q. Wang, Beyond symmetries: Anomalies in transverse Ward-Takahashi identities, Phys. Rev. D **102**, 056008 (2020).

[40] C.-B. Luo and H.-S. Zong, Transverse Ward-Takahashi identities and full vertex functions in different representations of QED_3, Chin. Phys. C **44**, 073105 (2020).

[41] A. I. Davydychev, P. Osland, and L. Saks, Quark gluon vertex in arbitrary gauge and dimension, Phys. Rev. D **63**, 014022 (2000).

[42] A. Bashir, A. Kizilersu, and M. R. Pennington, Analytic form of the one loop vertex and of the two loop fermion propagator in three-dimensional massless QED, arXiv: hep-ph/9907418.

[43] A. Bashir, A. Kizilersu, and M. R. Pennington, Does the weak coupling limit of the Burden-Tjiang deconstruction of the massless quenched three-dimensional QED vertex agree with perturbation theory?, Phys. Rev. D **62**, 085002 (2000).

[44] A. Bashir, Y. Concha-Sanchez, and R. Delbourgo, 3-point off-shell vertex in scalar QED in arbitrary gauge and dimension, Phys. Rev. D **76**, 065009 (2007).

[45] A. Bashir, A. Raya, and S. Sanchez-Madrigal, Chiral symmetry breaking and confinement beyond rainbow-ladder truncation, Phys. Rev. D **84**, 036013 (2011).

[46] L. Chang, C. D. Roberts, and P. C. Tandy, Selected highlights from the study of mesons, Chin. J. Phys. **49**, 955 (2011).

[47] G. Eichmann, H. Sanchis-Alepuz, R. Williams, R. Alkofer, and C. S. Fischer, Baryons as relativistic three-quark bound states, Prog. Part. Nucl. Phys. **91**, 1 (2016).

[48] G. Eichmann, C. S. Fischer, and H. Sanchis-Alepuz, Light baryons and their excitations, Phys. Rev. D **94**, 094033 (2016).

[49] S.-X. Qin, C. D. Roberts, and S. M. Schmidt, Ward-Green-Takahashi identities and the axial-vector vertex, Phys. Lett. B **733**, 202 (2014).

[50] P. Maris and P. C. Tandy, Bethe-Salpeter study of vector meson masses and decay constants, Phys. Rev. C **60**, 055214 (1999).

[51] A. C. Aguilar and A. A. Natale, A dynamical gluon mass solution in a coupled system of the Schwinger-Dyson equations, J. High Energy Phys. 08 (2004) 057.

[52] A. Cucchieri and T. Mendes, What's up with IR gluon and ghost propagators in Landau gauge? A puzzling answer from huge lattices, Proc. Sci., LAT2007 (**2007**) 297.

[53] I. L. Bogolubsky, E. M. Ilgenfritz, M. Muller-Preussker, and A. Sternbeck, The Landau gauge gluon and ghost propagators in 4D SU(3) gluodynamics in large lattice volumes, Proc. Sci., LAT2007 (**2007**) 290.

[54] A. Cucchieri and T. Mendes, Numerical test of the Gribov-Zwanziger scenario in Landau gauge, Proc. Sci., QCD-TNT09 (**2009**) 026.

[55] I. L. Bogolubsky, E. M. Ilgenfritz, M. Muller-Preussker, and A. Sternbeck, Lattice gluodynamics computation of Landau gauge Green's functions in the deep infrared, Phys. Lett. B **676**, 69 (2009).

[56] A. C. Aguilar, D. Binosi, and J. Papavassiliou, Gluon and ghost propagators in the Landau gauge: Deriving lattice results from Schwinger-Dyson equations, Phys. Rev. D **78**, 025010 (2008).

[57] P. Boucaud, J. P. Leroy, A. Le Yaouanc, J. Micheli, O. Pene, and J. Rodríguez-Quintero, On the IR behavior of the Landau-gauge ghost propagator, J. High Energy Phys. 06 (2008) 099.

[58] C. S. Fischer, A. Maas, and J. M. Pawlowski, On the infrared behavior of Landau gauge Yang-Mills theory, Ann. Phys. (Amsterdam) **324**, 2408 (2009).

[59] A. C. Aguilar, D. Binosi, J. Papavassiliou, and J. Rodriguez-Quintero, Nonperturbative comparison of QCD effective charges, Phys. Rev. D **80**, 085018 (2009).
[60] M. R. Pennington and D. J. Wilson, Are the dressed gluon and ghost propagators in the Landau gauge presently determined in the confinement regime of QCD?, Phys. Rev. D **84**, 119901 (2011).
[61] A. Blum, M. Q. Huber, M. Mitter, and L. von Smekal, Gluonic three-point correlations in pure Landau gauge QCD, Phys. Rev. D **89**, 061703 (2014).
[62] A. K. Cyrol, L. Fister, M. Mitter, J. M. Pawlowski, and N. Strodthoff, Landau gauge Yang-Mills correlation functions, Phys. Rev. D **94**, 054005 (2016).
[63] M. Q. Huber, On nonprimitively divergent vertices of Yang-Mills theory, Eur. Phys. J. C **77**, 733 (2017).
[64] D. Dudal, S. P. Sorella, N. Vandersickel, and H. Verschelde, New features of the gluon and ghost propagator in the infrared region from the Gribov-Zwanziger approach, Phys. Rev. D **77**, 071501 (2008).
[65] D. Dudal, J. A. Gracey, S. P. Sorella, N. Vandersickel, and H. Verschelde, A refinement of the Gribov-Zwanziger approach in the Landau gauge: Infrared propagators in harmony with the lattice results, Phys. Rev. D **78**, 065047 (2008).
[66] D. Dudal, O. Oliveira, and N. Vandersickel, Indirect lattice evidence for the refined Gribov-Zwanziger formalism and the gluon condensate $\langle A^2 \rangle$ in the Landau gauge, Phys. Rev. D **81**, 074505 (2010).
[67] J. M. Cornwall, Dynamical mass generation in continuum QCD, Phys. Rev. D **26**, 1453 (1982).
[68] P. O. Bowman, U. M. Heller, D. B. Leinweber, M. B. Parappilly, A. Sternbeck, L. von Smekal, A. G. Williams, and J.-b. Zhang, Scaling behavior and positivity violation of the gluon propagator in full QCD, Phys. Rev. D **76**, 094505 (2007).
[69] A. Ayala, A. Bashir, D. Binosi, M. Cristoforetti, and J. Rodriguez-Quintero, Quark flavor effects on gluon and ghost propagators, Phys. Rev. D **86**, 074512 (2012).
[70] A. C. Aguilar, D. Binosi, and J. Papavassiliou, Unquenching the gluon propagator with Schwinger-Dyson equations, Phys. Rev. D **86**, 014032 (2012).
[71] A. Bashir, A. Raya, and J. Rodriguez-Quintero, QCD: Restoration of chiral symmetry and deconfinement for large N_f, Phys. Rev. D **88**, 054003 (2013).
[72] D. Binosi, C. Mezrag, J. Papavassiliou, C. D. Roberts, and J. Rodriguez-Quintero, Process-independent strong running coupling, Phys. Rev. D **96**, 054026 (2017).
[73] Z.-F. Cui, J.-L. Zhang, D. Binosi, F. de Soto, C.. Mezrag, J. Papavassiliou, C. D. Roberts, J. Rodríguez-Quintero, J. Segovia, and S. Zafeiropoulos, Effective charge from lattice QCD, Chin. Phys. C **44**, 083102 (2020).
[74] A. Cucchieri, T. Mendes, and E. M. S. Santos, Covariant Gauge on the Lattice: A New Implementation, Phys. Rev. Lett. **103**, 141602 (2009).
[75] P. Boucaud, F. De Soto, K. Raya, J. Rodríguez-Quintero, and S. Zafeiropoulos, Discretization effects on renormalized gauge-field Green's functions, scale setting and gluon mass, Phys. Rev. D **98**, 114515 (2018).
[76] W. Kern, M. Q. Huber, and R. Alkofer, Spectral dimension as a tool for analyzing nonperturbative propagators, Phys. Rev. D **100**, 094037 (2019).
[77] L. Chang, I. C. Cloet, J. J. Cobos-Martinez, C. D. Roberts, S. M. Schmidt, and P. C. Tandy, Imaging Dynamical Chiral Symmetry Breaking: Pion Wave Function on the Light Front, Phys. Rev. Lett. **110**, 132001 (2013).
[78] F. Gao, S.-X. Qin, C. D. Roberts, and J. Rodriguez-Quintero, Locating the Gribov horizon, Phys. Rev. D **97**, 034010 (2018).
[79] S.-X. Qin, C. D. Roberts, and S. M. Schmidt, Poincaré-covariant analysis of heavy-quark baryons, Phys. Rev. D **97**, 114017 (2018).
[80] S.-X. Qin, C. D. Roberts, and S. M. Schmidt, Spectrum of light- and heavy-baryons, Few-Body Syst. **60**, 26 (2019).
[81] T. Nguyen, A. Bashir, C. D. Roberts, and P. C. Tandy, Pion and kaon valence-quark parton distribution functions, Phys. Rev. C **83**, 062201 (2011).
[82] M. Ding, K. Raya, D. Binosi, L. Chang, C. D. Roberts, and S. M. Schmidt, Symmetry, symmetry breaking, and pion parton distributions, Phys. Rev. D **101**, 054014 (2020).
[83] L. Chang, I. C. Cloët, C. D. Roberts, S. M. Schmidt, and P. C. Tandy, Pion Electromagnetic Form Factor at Spacelike Momenta, Phys. Rev. Lett. **111**, 141802 (2013).
[84] K. Raya, L. Chang, A. Bashir, J. J. Cobos-Martinez, L. X. Gutiérrez-Guerrero, C. D. Roberts, and P. C. Tandy, Structure of the neutral pion and its electromagnetic transition form factor, Phys. Rev. D **93**, 074017 (2016).
[85] G. Eichmann, C. S. Fischer, E. Weil, and R. Williams, On the large-Q^2 behavior of the pion transition form factor, Phys. Lett. B **774**, 425 (2017).
[86] K. Raya, M. Ding, A. Bashir, L. Chang, and C. D. Roberts, Partonic structure of neutral pseudoscalars via two photon transition form factors, Phys. Rev. D **95**, 074014 (2017).
[87] M. Ding, K. Raya, A. Bashir, D. Binosi, L. Chang, M. Chen, and C. D. Roberts, $\gamma^*\gamma \to \eta, \eta'$ transition form factors, Phys. Rev. D **99**, 014014 (2019).
[88] K. Raya, A. Bashir, and P. Roig, Contribution of neutral pseudoscalar mesons to a_μ^{HLbL} within a Schwinger-Dyson equations approach to QCD, Phys. Rev. D **101**, 074021 (2020).
[89] G. Eichmann, C. S. Fischer, and R. Williams, Kaon-box contribution to the anomalous magnetic moment of the muon, Phys. Rev. D **101**, 054015 (2020).
[90] G. Eichmann, C. S. Fischer, E. Weil, and R. Williams, Single pseudoscalar meson pole and pion box contributions to the anomalous magnetic moment of the muon, Phys. Lett. B **797**, 134855 (2019); Erratum, Phys. Lett. B **799**, 135029 (2019)].
[91] T. Aoyama *et al.*, The anomalous magnetic moment of the muon in the standard model, Phys. Rep. **887**, 1 (2020).
[92] J. C. Ward, An identity in quantum electrodynamics, Phys. Rev. **78**, 182 (1950).
[93] H. S. Green, A pre-renormalized quantum electrodynamics, Proc. Phys. Soc. London Sect. A **66**, 873 (1953).
[94] E. S. Fradkin, Concerning some general relations of quantum electrodynamics, Zh. Eksp. Teor. Fiz. **29**, 258 (1955).
[95] Y. Takahashi, On the generalized Ward identity, Nuovo Cimento **6**, 371 (1957).
[96] L. Chang, Y.-X. Liu, and C. D. Roberts, Dressed-Quark Anomalous Magnetic Moments, Phys. Rev. Lett. **106**, 072001 (2011).

[97] L. Chang and C. D. Roberts, Tracing masses of ground-state light-quark mesons, Phys. Rev. C **85**, 052201 (2012).
[98] A. Kizilersu, M. Reenders, and M. R. Pennington, One loop QED vertex in any covariant gauge: Its complete analytic form, Phys. Rev. D **52**, 1242 (1995).
[99] A. Kizilersu, T. Sizer, and A. G. Williams, Strongly coupled unquenched QED4 propagators using Schwinger-Dyson equations, Phys. Rev. D **88**, 045008 (2013).
[100] R. Williams, C. S. Fischer, and M. R. Pennington, Anti-q q condensate for light quarks beyond the chiral limit, Phys. Lett. B **645**, 167 (2007).
[101] S. J. Brodsky, C. D. Roberts, R. Shrock, and P. C. Tandy, Essence of the vacuum quark condensate, Phys. Rev. C **82**, 022201 (2010).
[102] L. Chang, C. D. Roberts, and P. C. Tandy, Expanding the concept of in-hadron condensates, Phys. Rev. C **85**, 012201 (2012).
[103] C. D. Roberts and A. G. Williams, Dyson-Schwinger equations and their application to hadronic physics, Prog. Part. Nucl. Phys. **33**, 477 (1994).
[104] F. E. Serna, Chen Chen, and Bruno El-Bennich, Interplay of dynamical and explicit chiral symmetry breaking effects on a quark, Phys. Rev. D **99**, 094027 (2019).
[105] C. D. Roberts, Electromagnetic pion form-factor and neutral pion decay width, Nucl. Phys. **A605**, 475 (1996).
[106] A. C. Aguilar, D. Binosi, and J. Papavassiliou, QCD effective charges from lattice data, J. High Energy Phys. 07 (2010) 002.
[107] Y.-Z. Xu, D. Binosi, Z.-F. Cui, B.-L. Li, C. D. Roberts, S.-S. Xu, and H. S. Zong, Elastic electromagnetic form factors of vector mesons, Phys. Rev. D **100**, 114038 (2019).
[108] Y. Lu, C. Chen, C. D. Roberts, J. Segovia, S.-S. Xu, and H.-S. Zong, Parity partners in the baryon resonance spectrum, Phys. Rev. C **96**, 015208 (2017).
[109] J. Segovia, B. El-Bennich, E. Rojas, I. C. Cloet, C. D. Roberts, S.-S. Xu, and H.-S. Zong, Completing the Picture of the Roper Resonance, Phys. Rev. Lett. **115**, 171801 (2015).
[110] K. Raya, L. X. Gutiérrez, and A. Bashir, Structure of the orbital excited N^* from the Schwinger-Dyson equations, Few-Body Syst. **59**, 89 (2018).